High-dimensional entanglement-enabled holography for quantum encryption

Ling-Jun Kong
Beijing Institute of Technology
Furong Zhang
Beijing Institute of Technology
Jingfeng Zhang
Beijing Institute of Technology
Yifan Sun
Beijing Institute of Technology
Xiangdong Zhang (zhangxd@bit.edu.cn)
Beijing Institute of Technology

Letter

Keywords: cryptography, quantum encryption, holography

Posted Date: July 12th, 2021

DOI: https://doi.org/10.21203/rs.3.rs-658825/v1

High-dimensional entanglement-enabled holography for quantum encryption

Ling-Jun Kong, Furong Zhang, Jingfeng Zhang, Yifan Sun, and Xiangdong Zhang*

Key Laboratory of advanced optoelectronic quantum architecture and measurements of Ministry of Education, Beijing Key Laboratory of Nanophotonics & Ultrafine Optoelectronic Systems, School of Physics, Beijing Institute of Technology, 100081 Beijing, China.

**Author to whom any correspondence should be addressed: zhangxd@bit.edu.cn*

Cryptography plays an important role in information security, which is widely applied in the various fields of society. Quantum cryptography has shown its great advantages in information security compared with the classical one[1]. Two major directions of quantum cryptography are quantum key distribution (QKD) and quantum encryption, with the former focusing on secure key distribution[2–6] and the latter focusing on encryption using quantum algorithms[7–10]. In contrast to the well accepted success of the QKD[11–15], the development of quantum encryption is rather limited because of the difficulties of building up algorithms and the constructing the practical quantum computers. Here we propose a new scheme of quantum encryption based on high-dimensional entanglement holography. Firstly, we experimentally realize the quantum holography based on the high-dimensional orbital angular momentum (OAM) entanglement. Then, OAM-selective holographic scheme for quantum encryption is proposed and demonstrated. Our results show that introducing quantum entangled state into OAM holography makes the OAM holography possess infinite information channels and the transmission of information be absolute security in principle. Furthermore, decryption in the presence of strong noise is achieved. Our work opens up a new way to realize quantum information security.

The developed all-optical holographic encryption shows great potential for information security[16–18]. In the holographic encryption, the level of security of information transmission depends on the dimension of the degree of freedom used, which corresponds to the number of information channels. Orbital angular momentum (OAM)[19–24], as a novel degree of freedom of photons, can be used for representing the state vector of an infinite dimensional Hilbert space in principle. Recently, Ren et al. proposed a strong OAM selectivity method in the spatial-frequency domain and realized the OAM holography, where the OAM states have been used for encoding information. They also achieved ultrahigh-capacity holographic multiplexing and high-security encryption[17].

On the other hand, quantum encryption has attracted great attention due to its advantages in information

security[7–10]. The problem is whether a quantum advance can be found for encryption, comparing with the corresponding all-optical OAM holographic classical scheme. To realize such a quantum encryption scheme, the quantum holography based on the high-dimensional OAM entanglement has to be implemented at first. Hologram has been introduced into the quantum optics[25–27], and observed with single photons[28] or polarization entangled state[29]. However, the realization of the high-dimensional OAM entanglement holography is still a great challenge. In this work, we firstly construct such a quantum OAM holographic system, then, apply it into encryption scheme and achieve higher-security quantum encryption.

The conceptual arrangement of our high-dimensional quantum OAM holographic scheme is illustrated in Fig. 1a. The high-dimensional OAM entangled state of photon-pair is described as $|\Psi\rangle=\sum_{l=-\infty}^{l=+\infty} c_l|l\rangle_A|-l\rangle_B$. Here, $|l\rangle$ denotes a state of photon with an OAM of $l\hbar$. Subscript A (B) labels the optical path-A (B). c_l represents the amplitude of the lth-order OAM state. After interacting with a spatial light modulator (SLM-A), photon-A is coupled into a single mode fiber (SMF) and then detected by a single photon detector (D-A). Because only fundamental Gaussian mode state (e.g, OAM state $|0\rangle$) can be coupled into the SMF, the combination of SLM-A and SMF can implement the OAM projection operator described by $\hat{P}_A$. The SLM-B is used for displaying the holographic phase pattern and its function for photon-B is described by an operator $\hat{P}_B^{\mathrm{H}}$. After interacting with the SLM-B and being transformed to the Fourier space by lens Lf, the photon-B is collected by a multimode fiber (MMF) and detected by another single photon detector (D-B). The input of the MMF need to be the intensity of all locations of the Fourier plane of Lf, which can be obtained by scanning the plane point-by-point. Thus, the holographic image with coincidence measurement between D-A and D-B is calculated as

$$H_i = \left|\mathrm{F}\left(\hat{P}_B^{\mathrm{H}}\hat{P}_A|\Psi\rangle\right)\right|^2. \tag{1}$$

Here, $\mathrm{F}(\cdot)$ represents the Fourier transformation.

To realize such a quantum holography, the OAM-selective hologram should be displayed on the SLM-B. The OAM-selective hologram is obtained by encoding an OAM state $|l_{\mathrm{e}}\rangle$ onto an OAM-preserved hologram, which is generated by multiplying a target image with a sampling array (see S1 in Supplementary Information for details). An example is shown in the right side of Fig. 1a, where the target is the image of the letters “BIT”, the phase distribution of the OAM-preserved hologram is described with φ and $l_{\mathrm{e}}=1$. In such a case, the function of the operator for photon-B is expressed as $\hat{P}_B^{\mathrm{H}}|l\rangle_B = e^{j\varphi}|l_{\mathrm{e}}+l\rangle_B = e^{j\varphi}|1+l\rangle_B$. By setting the specific phase patterns of the SLM-A OAM, which corresponds to the projection operator $\hat{P}_A=\langle 2|_A$, $\langle 1|_A$, $\langle -1|_A$, and $\langle -2|_A$, the quantum OAM-selective holographic images can be calculated by Eq. (1). The

experiment has been carried out. The experimental results are given in Fig.1b, and the corresponding simulation results are shown in Fig. S2 of Supplementary Information. Because the OAM state encoded by the OAM-selective hologram is $|1\rangle$, only the given OAM projection operator $\hat{P}_A=\langle 1|_A$ can convert each pixel of the holographic image into the Gaussian mode, i.e., $\hat{P}_B^{\mathrm{H}}\hat{P}_A|\Psi\rangle \propto \hat{P}_B^{\mathrm{H}}|-1\rangle_B = e^{j\varphi}|0\rangle_B$. In the OAM-selective holographic experiment, only the Gaussian mode contributes to the reconstruction of holographic image (see S3 in Supplementary Information for details). It is seen clearly that the OAM-selective holographic image can only be reconstructed for $\hat{P}_A=\langle 1|_A$ with signal-to-noise ratio (SNR)~16.0. Here the value of SNR can describe the clarity of the image, which the detailed discussion is given in Methods. The agreements between experimental and theoretical results are very well, which means that the high-dimensional OAM entanglement-enabled holography has been realized.

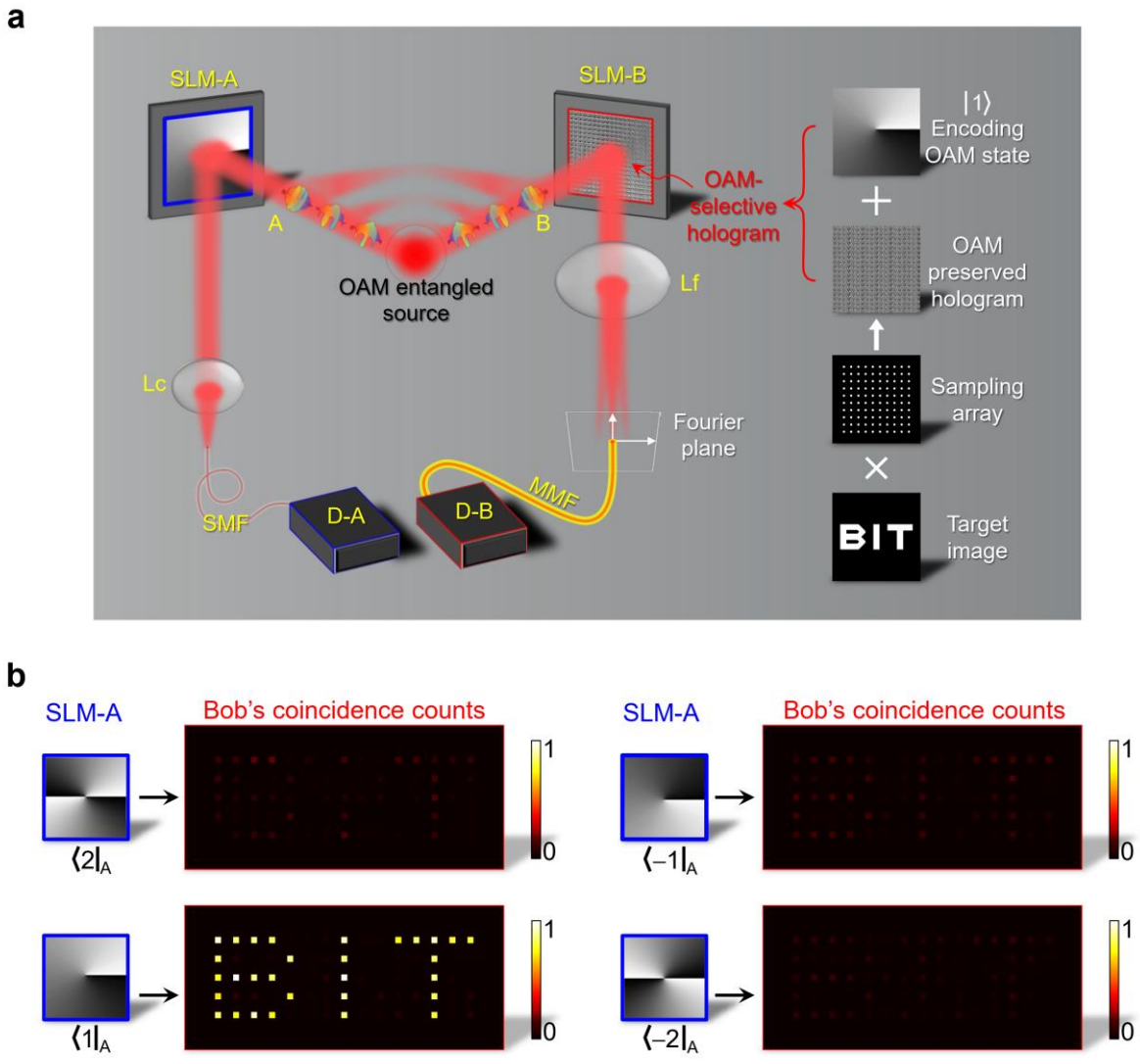

Fig. 1 | High-dimensional OAM entanglement-enabled quantum holography. a, Schematic illustration of setup. Photon-A(B) of each entangled photon pair in high-dimensional OAM states propagates through the

spatial light modulator SLM-A (SLM-B), is then coupled into SMF (MMF), and detected by D-A (D-B). SMF and MMF represent single mode fiber and multi-mode fiber (with core diameter 25μm), respectively. D-A and D-B are two single photon detectors. The lenses Lc and Lf are applied for collecting photon-A and implementing Fourier transformation for photon-B, respectively. A two-axis stage is used for scanning the input end of the MMF in the Fourier plane of Lf. Right side shows the design of the OAM preserved and OAM-selective hologram. **b**, Quantum OAM-selective holographic images reconstructed by coincidence measurement with the OAM projection operators $\hat{P}_A = \langle 2|_A$, $\langle 1|_A$, $\langle -1|_A$, and $\langle -2|_A$. There are 15×5=75 pixels in each reconstructed holographic image. The coincidence counts are normalized by the holographic image for the OAM projection $\hat{P}_A = \langle 1|_A$).

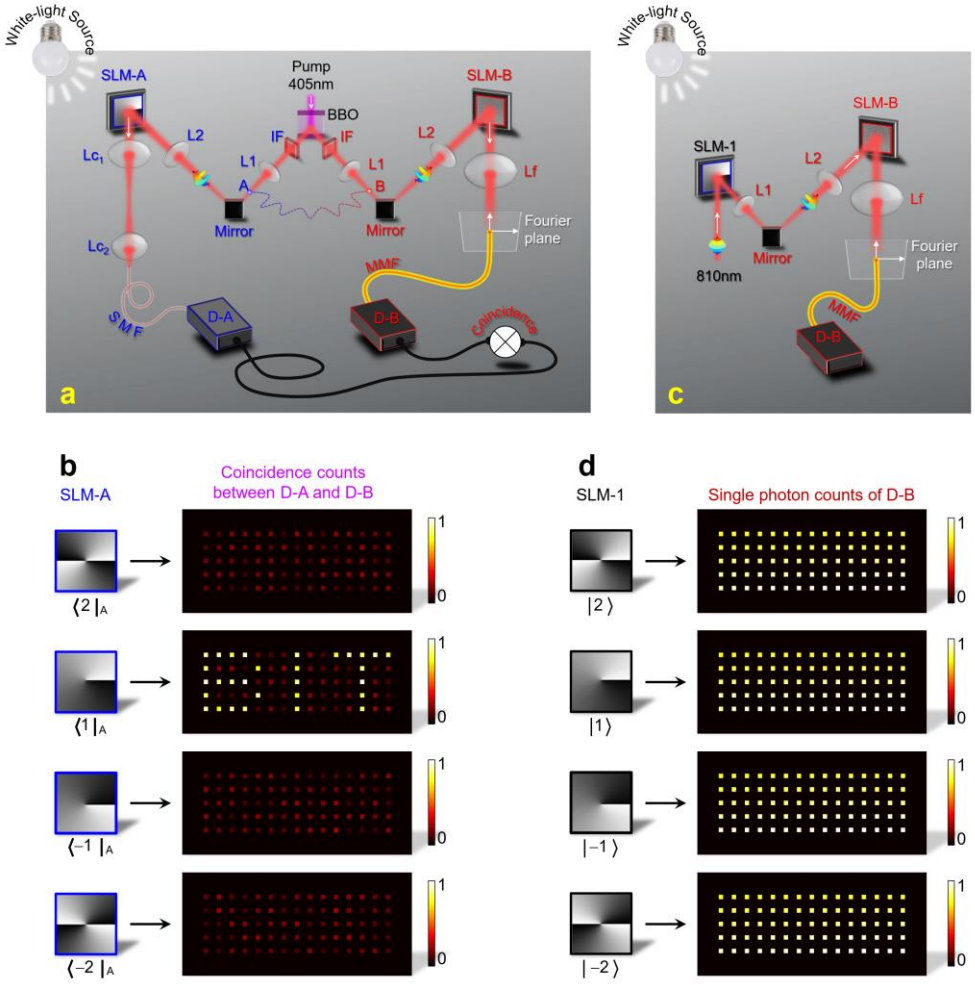

Fig. 2 | Quantum OAM-selective holography in the presence of classical noise. a, Experimental apparatus of quantum OAM-selective holographic system. Photon pairs entangled in high-dimensional OAM are produced by pumping a β-barium borate (BBO) crystal under type I spontaneous parametric down conversion. Behind BBO, unwanted photons are filtered out by an interference filter (IF) centered at 810 ± 3 nm in path-A and path-B. Lenses L1 and L2 implement a 4f system and image the plane of the BBO on the SLM-A and SLM-B. After interacting with SLM-A, photon-A is coupled into the SMF with collecting lenses (Lc_1 and Lc_2) and detected by D-A. After undergoing an optical Fourier transform implemented by lens Lf, photon-B is collected

by a MMF in the Fourier plane of Lf and detected by D-B. **c**, Experimental apparatus of classical OAM holographic system. A collimated light beam (810 nm) illuminates SLM-1 for generating incident OAM state. Lenses L1 and L2 image SLM-1 on SLM-B. OAM-selective holographic images measured by recording the counts of D-B in the presence of dynamic stray light for different incident OAM states. For comparison, SLM-B displays the same OAM-selective hologram used in the experiments of both quantum and classical OAM holographic system shown by Fig.1. **b** and **d**, OAM-selective holographic images obtained by quantum and classical OAM holographic systems, respectively. The letters "BIT" can only be obtained by our quantum OAM holographic systems with SNR~6 when the projection operator $\hat{P}_A=\langle l|_A$.

One of the advantages of quantum holography is its robustness to classical noise, as demonstrated by the recent experiments[30,31]. The holographic imaging of the amplitude objects is immune against the corruption induced by static stray light[30,31]. In order to test such an effect, we use white light of a lamp as classical noise in the experiment of quantum OAM holography as shown in Fig. 2a. The experimental results for reconstructing the OAM-selective holographic images are given in Fig. 2b. It is shown clearly that the encoded image (letters "BIT") can be accurately reconstructed for $\hat{P}_A=\langle l|_A$ in the presence of classical stray light, with only a lower SNR compared to the case without stray light (Fig. 1b). This benefits from the correlation properties of entangled photon pairs. In contrast, if we use single photon, instead of entangled photons, to reconstruct the holographic image as shown in Fig. 2c, the experimental results are provided in Fig. 2d. The images become too vague to tell the letters, no matter what kind of OAM state is used. That is to say, the noise destroys the holography in such a case. The phenomena are similar to the case for the polarization entanglement-enabled quantum holography[29]. The advantage of OAM in quantum holography is that it can greatly increase the channel capacity and improve the confidentiality of information transmission.

What's exciting is that the introduction of quantum entanglement can enable all-optical quantum OAM-selective holographic encryption with a higher level of security compared with that in classical system. As is well known, a classical bit would have to be in one state or the other. However, a qubit is allowed to be in a coherent superposition of both states. Here, we take the OAM states $|l\rangle$ and $|-l\rangle$ as an example. In the first-order OAM Poincaré sphere as shown in Fig. 3a, $|l\rangle$ and $|-l\rangle$ are located at north and south poles, respectively[32,33]. Any state of superposition of $|l\rangle$ and $|-l\rangle$ can be described by a point on the Poincaré sphere. The points on the equator, for instance, represents the superposition of $|l\rangle$ and $|-l\rangle$ with equal probabilities; the relative phase of the superposition determines the orientation of the dark lines produced by coherent cancellation. In our quantum OAM holographic system, the information can be encoded by any point on the Poincaré sphere in principle, which implies that the introduction of quantum superposition state leads to the infinite information channels and absolute confidentiality of information in principle. While, in classical

OAM holographic system, the information is encoded with the north ($|l\rangle$) or south pole ($|-l\rangle$), only two information channels[17].

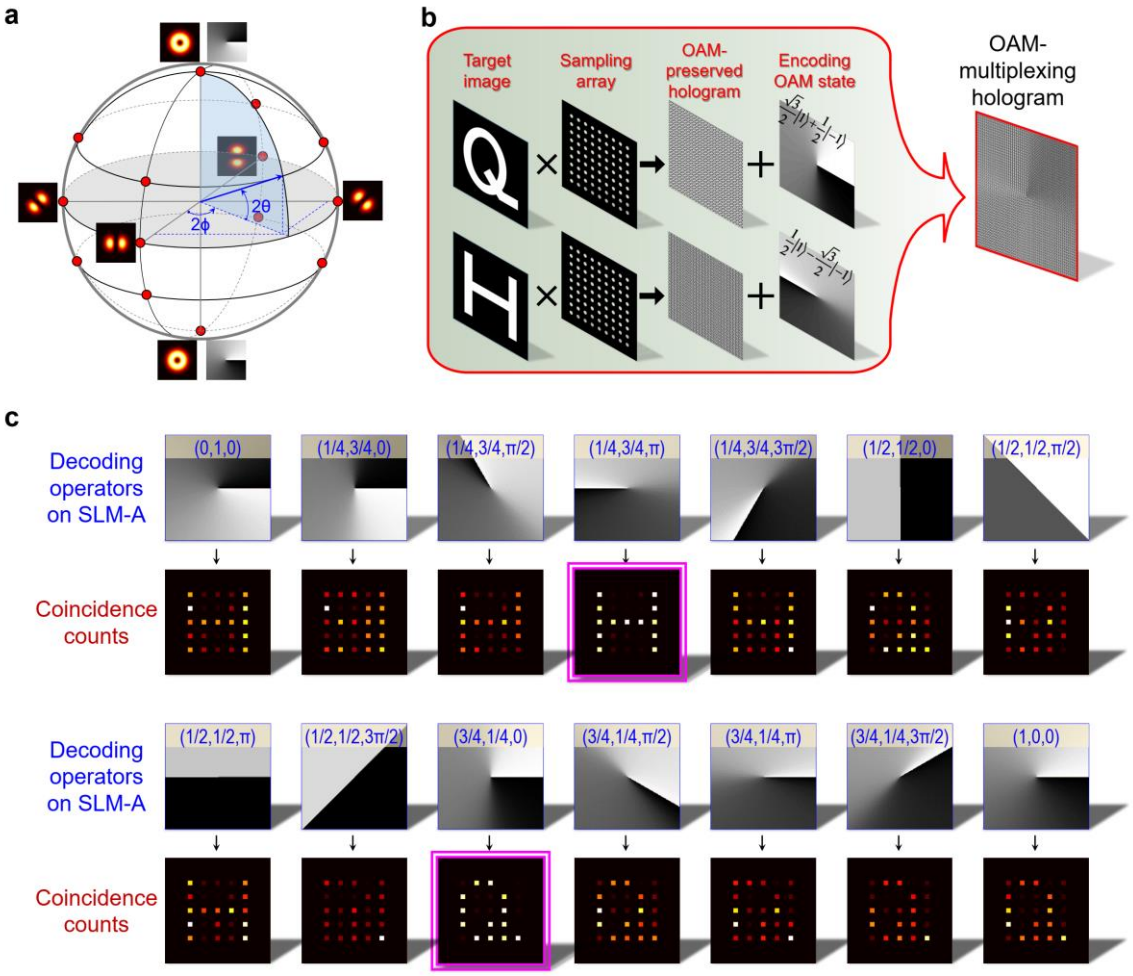

Fig. 3 | High-security quantum holographic encryption based on OAM entangled state. a, The Poincaré sphere representing the OAM state space spanned by $\{|l\rangle, |-l\rangle\}$. Its north and south poles represent the $|l\rangle$ and $|-l\rangle$. Any superposition state of $|l\rangle$ and $|-l\rangle$ can be represented by a point on the Poincaré sphere, which is located by two angle parameters $\theta \in [-\pi/4, \pi/4]$ and $\phi \in [0, \pi]$. Thus, the whole sphere represents a qubit. **b**, Design of OAM-multiplexing hologram based on OAM superposition states. **c**, Experimental OAM-selective holographic images obtained with coincidence measurement for different decoding operators implemented on SLM-A.

Considering the fact that there are infinite superposition states, it is impossible to verify them one by one experimentally. To prove our idea in experiment without losing generality, we firstly choose fourteen discrete superposition states for two-dimensional case, which correspond to the fourteen red points on the Poincaré sphere (Fig. 3a). To implement quantum encryption, OAM-multiplexing holography should be realized in our quantum system first (See S4 in Supplementary Information for detail). As shown in Fig. 3b, two OAM-preserved holograms are obtained by multiplying two target images (letters 'Q' and 'H') with a sampling array,

respectively. Then two OAM superposition states, $(\sqrt{3}|1\rangle+|-1\rangle)/2$ and $(|1\rangle-\sqrt{3}|-1\rangle)/2$, are encoded into the OAM-preserved holograms for generating two OAM-selective holograms, respectively. The OAM-multiplexing hologram is achieved by combining the two OAM-selective holograms. Fig. 3c shows the experimental OAM-selective holographic images obtained with different decoding operators. The decoding operators implemented by the SLM-A are described by $\hat{P}_A=\sqrt{a_1}\langle 1|_A+\sqrt{a_2}e^{-j\phi_1}\langle -1|_A$, where non-negative a_1 and a_2 represent intensities and satisfy the normalized condition $a_1+a_2=1$, ϕ_1 represents relative phase. The values of parameters (a_1, a_2, ϕ_1) are listed on each decoding operator. It is confirmed that the images of letters 'Q' and 'H' can be detected with (a_1, a_2, ϕ_1) = (3/4, 1/4, 0) and (1/4, 3/4, π) (marked with the frames of purple line in Fig. 3c) with SNR=14.4 and 13.4, respectively.

In order to avoid the crosstalk of the information, the superposition states encoded into the multiplexing hologram should be orthogonal to each other. In fact, the high dimension of the OAM entangled states provides a natural advance. The more basis vectors one introduces for information encoding, the more complicated information representation one can obtain, and the harder it is for others to find the vital message hidden in the high dimensional space. As shown in Fig. 4a, four OAM-preserved holograms are obtained by multiplying four target images (letters 'O', 'A' , 'M', and 'H') with a sampling array, respectively. Then four OAM superposition states, $(|1\rangle+|-1\rangle)/\sqrt{2}$, $(|1\rangle-|-1\rangle)/\sqrt{2}$, $(|2\rangle+j|-2\rangle)/\sqrt{2}$, and $(|2\rangle-j|-2\rangle)/\sqrt{2}$, are encoded into the OAM-preserved holograms for generating four OAM-selective holograms, respectively. The OAM-multiplexing hologram is achieved by combining these OAM-selective holograms and displays on the SLM-B. Correspondingly, there is an infinite number of OAM-selective holographic images for decoding operators. As examples, Fig. 4b displays the experimental results of OAM-selective holographic images for twenty-eight kinds of decoding operators. The decoding operators are implemented by the SLM-A, which are described as $\hat{P}_A=\sqrt{a_1}\langle -1|_A+\sqrt{a_2}e^{-j\phi_1}\langle 1|_A+\sqrt{a_3}e^{-j\phi_2}\langle -2|_A+\sqrt{a_4}e^{-j\phi_3}\langle 2|_A$. Here, non-negative a_1, a_2, a_3, and a_4 represent intensities and satisfy the normalized condition $a_1+a_2+a_3+a_4=1$, where ϕ_1, ϕ_2, and ϕ_3 are the relative phases. The values of parameters (a_1, a_2, a_3, a_4, ϕ_1, ϕ_2, ϕ_3) are listed on each reconstructed OAM-selective holographic image with h=1/2, $\alpha=\pi/2$, $\beta=\pi$ and $\gamma=3\pi/2$. The images of letters 'O', 'A', 'M', and 'H' can be decoded with (a_1, a_2, a_3, a_4, ϕ_1, ϕ_2, ϕ_3) = (1/2, 1/2, 0, 0, 0, 0, 0), (1/2, 1/2, 0, 0, π, 0, 0), (0, 0, 1/2, 1/2, 0, 0, $\pi/2$), and (0, 0, 1/2, 1/2, 0, 0, $3\pi/2$) (marked with the frames of purple line) with SNR=11.4, 11.1, 12.6, and 11.9, respectively. More conditions have been tested in the experiment (See S5 in Supplementary Information).

Successful encryption and decryption using the OAM-selective quantum holographic scheme has been demonstrated again. As we all know, to uniquely identify an unknown d-dimensional entangled state, one should carry out the standard quantum tomography[34,35], where the required number of measurements increase with the dimension of entangled state as ~O(d^4). This means that the higher dimension of the OAM entangled state, the higher security of information transmission.

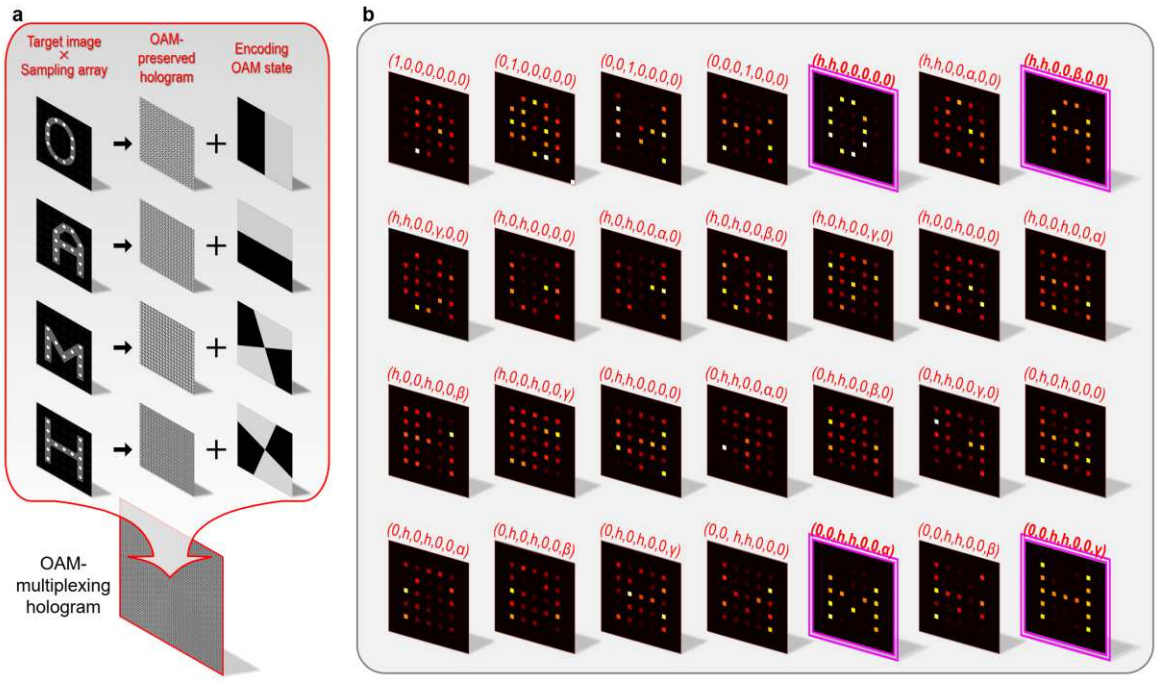

Fig. 4 | High-security holographic encryption based on high-dimensional OAM entangled states. a, Design of multiplexing hologram based on OAM superposition states and its corresponding OAM-multiplexing hologram displaying on SLM-B. **b**, Experimental OAM-selective holographic images for different decoding operators implemented with SLM-A.

In conclusion, we have realized the quantum holography based on high-dimensional OAM entanglement for the first time, and demonstrated a new scheme of quantum encryption based on such a holography. In the quantum OAM holography, the information can be encoded by the superposition states of OAM modes, which leads to the infinite information channels, and the information transmission is regarded as absolute security in principle. In the experiments, the two and four-dimensional cases of our proposal have been implemented, verifying the idea. The introduction of entanglement not only allows us to reconstruct the holographic images remotely and enhance the manipulation of information transmission, but also effectively reduces the impact of classical noise. The decryption in the presence of strong noise has been achieved. With the rapid development of the faster and cheaper sensors for imaging quantum correlations, our quantum OAM holography shows great potentials in quantum optical communications and opens up a new way for quantum information security.

Online content

Any methods, additional references, Nature Research reporting summaries, source data, extended data, supplementary information, acknowledgements, peer review information; details of author contributions and competing interests; and statements of data and code availability are available at https:xxx

References

1. Gisin, N., Ribordy, G., Tittel, W. & Zbinden, H. Quantum cryptography. *Rev. Mod. Phys.* **74**, 145–195 (2002).
2. Bennett, C. H. & Brassard, G. Quantum cryptography: Public key distribution and coin tossing. *Theoretical Computer Science* **560**, 7–11 (2014).
3. Ekert, A. K. Quantum cryptography based on Bell's theorem. *Phys. Rev. Lett.* **67**, 661–663 (1991).
4. Bennett, C. H., Brassard, G. & Mermin, N. D. Quantum cryptography without Bell's theorem. *Phys. Rev. Lett.* **68**, 557–559 (1992).
5. Peng, C.-Z. *et al.* Experimental Long-Distance Decoy-State Quantum Key Distribution Based on Polarization Encoding. *Phys. Rev. Lett.* **98**, 010505 (2007).
6. Rosenberg, D. *et al.* Long-Distance Decoy-State Quantum Key Distribution in Optical Fiber. *Phys. Rev. Lett.* **98**, 010503 (2007).
7. Zhou, R.-G., Wu, Q., Zhang, M.-Q. & Shen, C.-Y. Quantum Image Encryption and Decryption Algorithms Based on Quantum Image Geometric Transformations. *Int. J. Theor. Phys.* **52**, 1802–1817 (2013).
8. Zhou, N. R., Hua, T. X., Gong, L. H., Pei, D. J. & Liao, Q. H. Quantum image encryption based on generalized Arnold transform and double random-phase encoding. *Quantum Inf. Process.* **14**, 1193–1213 (2015).
9. Ran, Q., Wang, L., Ma, J., Tan, L. & Yu, S. A quantum color image encryption scheme based on coupled hyper-chaotic Lorenz system with three impulse injections. *Quantum Inf. Process.* **17**, 188 (2018).
10. Jiang, N., Dong, X., Hu, H., Ji, Z. & Zhang, W. Quantum Image Encryption Based on Henon Mapping. *Int. J. Theor. Phys.* **58**, 979–991 (2019).
11. Yin, H.-L. *et al.* Measurement-Device-Independent Quantum Key Distribution Over a 404 km Optical

Fiber. *Phys. Rev. Lett.* **117**, 190501 (2016).

12. Boaron, A. *et al.* Secure Quantum Key Distribution over 421 km of Optical Fiber. *Phys. Rev. Lett.* **121**, 190502 (2018).

13. Yin, J. *et al.* Entanglement-based secure quantum cryptography over 1,120 kilometres. *Nature* **582**, 501–505 (2020).

14. Peev, M. *et al.* The SECOQC quantum key distribution network in Vienna. *New J. Phys.* **11**, 075001 (2009).

15. Lo, H.-K., Curty, M. & Tamaki, K. Secure quantum key distribution. *Nat. Photon.* **8**, 595–604 (2014).

16. Ren, H. *et al.* Metasurface orbital angular momentum holography. *Nat. Commun.* **10**, 2986 (2019).

17. Fang, X., Ren, H. & Gu, M. Orbital angular momentum holography for high-security encryption. *Nat. Photon.* **14**, 102–108 (2020).

18. Jin, J. *et al.* Multi-Channel Vortex Beam Generation by Simultaneous Amplitude and Phase Modulation with Two-Dimensional Metamaterial. *Adv. Mater. Technol.* **2**, 1600201 (2017).

19. Allen, L., Beijersbergen, M. W., Spreeuw, R. J. C. & Woerdman, J. P. Orbital angular momentum of light and the transformation of Laguerre-Gaussian laser modes. *Phys. Rev. A* **45**, 8185–8189 (1992).

20. Mair, A., Vaziri, A., Weihs, G. & Zeilinger, A. Entanglement of the orbital angular momentum states of photons. *Nature* **412**, 313–316 (2001).

21. Zeng, Q., Wang, B., Li, P. & Zhang, X. Experimental High-Dimensional Einstein-Podolsky-Rosen Steering. *Phys. Rev. Lett.* **120**, 030401 (2018).

22. Malik, M. *et al.* Direct measurement of a 27-dimensional orbital-angular-momentum state vector. *Nat. Commun.* **5**, 3115 (2014).

23. Kong, L.-J. *et al.* Manipulation of eight-dimensional Bell-like states. *Sci. Adv.* **5**, eaat9206 (2019).

24. Shen, Y. *et al.* Optical vortices 30 years on: OAM manipulation from topological charge to multiple

singularities. *Light Sci. Appl.* **8**, 90 (2019).

25. Abouraddy, A. F., Saleh, B. E. A., Sergienko, A. V. & Teich, M. C. Quantum holography. *Opt. Express* **9**, 498–505 (2001).

26. Devaux, F., Mosset, A., Bassignot, F. & Lantz, E. Quantum holography with biphotons of high Schmidt number. *Phys. Rev. A* **99**, 033854 (2019).

27. Song, X.-B. *et al.* Experimental observation of one-dimensional quantum holographic imaging. *Appl. Phys. Lett.* **103**, 131111 (2013).

28. Chrapkiewicz, R., Jachura, M., Banaszek, K. & Wasilewski, W. Hologram of a single photon. *Nat. Photon.* **10**, 576–579 (2016).

29. Defienne, H., Ndagano, B., Lyons, A. & Faccio, D. Polarization entanglement-enabled quantum holography. *Nat. Phys.* **17**, 591–597 (2021).

30. Defienne, H., Reichert, M., Fleischer, J. W. & Faccio, D. Quantum image distillation. *Sci. Adv.* **5**, eaax0307 (2019).

31. Gregory, T., Moreau, P.-A., Toninelli, E. & Padgett, M. J. Imaging through noise with quantum illumination. *Sci. Adv.* **6**, eaay2652 (2020).

32. Padgett, M. J. & Courtial, J. Poincar´ e-sphere equivalent for light beams containing orbital angular momentum. *Opt. Lett.* **24**, 430–432 (1999).

33. Milione, G., Sztul, H. I., Nolan, D. A. & Alfano, R. R. Higher-Order Poincaré Sphere, Stokes Parameters, and the Angular Momentum of Light. *Phys. Rev. Lett.* **107**, 053601 (2011).

34. Agnew, M., Leach, J., McLaren, M., Roux, F. S. & Boyd, R. W. Tomography of the quantum state of photons entangled in high dimensions. *Phys. Rev. A* **84**, 062101 (2011).

35. Pan, J.-W. *et al.* Multiphoton entanglement and interferometry. *Rev. Mod. Phys.* **84**, 777–838 (2012).

Methods

Experimental layout. The pump light is a femtosecond pulsed laser polarized at 0° with a fundamental Gaussian mode, a power of ~600mW, a central wavelength of 405 nm, a pulse duration of ~140 fs, and a repetition rate of 80 MHz (Coherent chameleon). A β-barium borate (BBO) crystal with dimensions of 0.6×7×7 mm^3 were cut for producing down-converted photons at a degenerate wavelength of 810 nm in a ~3.0° half-opening angle cone under the type I phase-matching condition. A 650-nm-cutoff long-pass filter was used to block pump photons after the crystals (not shown in main text). There is an interference filter (IF) centred at 810 ± 3 nm in front of each single photon detectors (Perkin Elmer). The SLM was a phase-only modulator (Holoeye Pluto-2-NIR-015) with 1920×1080 pixels and a pixel pitch of 8μm. The focal length of lenses are as follows: L1, 200mm; L2, 500mm; Lc_1, 200mm; Lc_2, 11mm; Lf, 150mm. The distances between components were as follows: crystal plane to lens L1, 200 mm; lens L1 to Mirror, 200 mm; Mirror to lens L2, 500 mm; lens L2 to SLM, 500 mm; SLM-A to lens Lc_1, 200 mm; SLM-B to lens Lf, 150 mm; lens Lf to Fourier plane, 150 mm. The distance between Lc_1 and Lc_2 is dependent on the distance between Lc_2 and the input end of SMF for make sure that SLM-A is imaged onto the input end of SMF. Due to that the distance from Lc_2 to the input end of SMF too hard to be measured, the key point is to make sure that when we incident a beam of light from the output end of SMF reversely, light emitted from input end of SMF will be focus on the back focal plane of Lc_1 after passing Lc_2.

The SNR in experiments. The SNR is defined as $10\log_{10}(C_{Sig}/C_{Noise})$, where C_{Sig} and C_{Noise} represent the average coincidence counts of the desired and undesired pixels of OAM-selective holographic image, respectively. It is easy to obtain that when there is no signal, $C_{Sig} = C_{Noise}$, and thus SNR = 0; when there is no noise, $C_{Sig} = C_{Noise}$, and thus SNR = ∞. The value of SNR is affected by pump power, coincidence counting time, pixel number and so on. In our experiment, the pump power (~600 mW) and coincidence counting time (15s for each pixel) are fixed. In the presence of classical noise, the average coincidence counts of both the desired and undesired pixels will be increased by C_{CN}. Thus, the SNR decreases to be $10\log_{10}[(C_{Sig}+C_{CN})/(C_{Noise}+C_{CN})]$. For classical OAM holographic system (Fig. 1c), the $C_{CN} >> C_{Sig} >> C_{Noise}$, and thus SNR~0, which implies that the images will become too vague to tell the letters. While, for quantum OAM holographic system (Fig. 1a), the coincidence measurement decreases the C_{CN} greatly. Leading to $C_{Noise} < C_{CN} < C_{Sig}$, and thus SNR>3, which means that the images is still clear.

Data availability

The data that underlie the plots within this paper and other findings of this study are available from the corresponding authors on reasonable request.

Code availability

The code used to generate simulated data and plots is available from the corresponding authors on reasonable request.

Acknowledgements

This work was supported by the National key R & D Program of China under Grant No. 2017YFA0303800, National Natural Science Foundation of China (12004038 and 11904022).

Author contributions

L. J. K. provided the theoretical designs for the schemes of quantum OAM holography with the help of Y. F. S.. The experiments were performed by L. J. K. with the help of F. R. Z. and J. F. Z.. X. D. Z. initiated and designed this research project.

Competing interests

The authors declare no competing interests.

Additional information

Supplementary information The online version contains supplementary material available at https:xxx.

Correspondence and requests for materials should be addressed to X.D. Z..

Peer review information Nature Photonics thanks xxx.

Supplementary Files

This is a list of supplementary files associated with this preprint. Click to download.

- kongZhangFV09SI.pdf